# Impedance Identification Signal Excitation for Series-End Winding Motor System

Hongyan Qu[1], Boyang. Li[1], Min Zhou[1], Dong Jiang[1] and Wei Sun[1]
[1] Huazhong University of Science and Technology

***Abstract*-- At present, the study of battery impedance mainly focuses on off-line operating conditions, which cannot reflect the battery status online in real time. In this article, an online real-time battery impedance monitoring method is proposed with the traction inverter. This system allows superimposing an AC excitation signal of the desired frequency on the DC side without affecting the normal operation of the motor. Another advantage of this method is that no additional excitation device is needed. The amplitude and frequency of the signal are controlled by the motor drive system. Simulation and experiment are carried out to verify the feasibility of this novel method.**

***Index Terms*-- battery impedance identification, on-line impedance, series-end winding motor, signal processing**

## I. Introduction

High-level battery pack is used in a wide-range of industry fields. However, the safety of battery is the biggest concern in applications. Battery impedance is one of the important parameters to reflect battery temperature, state of charge, state of health, and malfunctions such as overcharge, over discharge, and short circuit. [1] Nevertheless, battery impedance is often obtained off-line. The off-line impedance of a battery is obtained by frequency sweeping through an electrochemical workstation. The disadvantage of this method is that it is not possible to monitor the impedance changes in operation, and needs extra equipment. Therefore, real-time monitoring is unachievable [2]. In previous studies, many scholars have used DC/DC converters to generate the necessary excitation for impedance identification, but few have studied inverters such as motor drive. [3-6]

In this article, a novel real-time excitation method based on series-end winding motor system is proposed, which can integrate real-time battery impedance identification with the traction drive. Series-end winding system has advantages of high-voltage output and wide speed range. Another feature of this structure is the possibility of injecting arbitrary zero-sequence currents in the motor. Thus, the freedom of current control is increased. The method and theoretical analysis are in part II. In part III, simulation and experiment are presented and analyzed. Some typical frequencies are chosen to illustrate the method. In part IV, a summary and outlook are presented.

## II. Method and Theoretical Analysis

### A. Introduction of series-end winding motor system

A series-end winding motor system is shown in Fig 1. The motor is an open-winding three-phase AC motor. The three phase windings are connected in series. The motor is controlled by a four-bridge converter. This structure can increase the maximum output voltage of the inverter to more than 70% compared to the three-phase half-bridge structure under the same DC voltage conditions [7]. This topology is with merit for EV traction.

The relationship between the output voltage of the inverter and the phase voltage of the motor is shown in (1). $V_i$ ($i$ = $a$,$b$,$c$) is phase voltage of the motor. $V_{li}$ ($i$ = 1,2,3,4) is output voltage of each phase. According to [7], the the output voltage of each bridge and the voltage in the dq0 coordinate have a transformation formula as (2). $\theta_e$ is electrical angle of the rotor. $V_{ld}$ and $V_{lq}$ are calculated from $V_d$ and $V_q$ by (3). $V_0$ is zero-sequence voltage. In the transformation matrix, the third column represents the output of zero sequence voltage. The output voltage of each bridge is [$-V_{dc}/2$, $V_{dc}/2$], and $V_0$ has a maximum value of $V_{dc}/3$ according to (2). It is worth noting that the maximum value can be obtained only when $V_d = V_q = 0$, otherwise the output voltage will exceed the linear modulation range.

$$\begin{cases} V_a = V_{l1} - V_{l2} \\ V_b = V_{l2} - V_{l3} \\ V_c = V_{l3} - V_{l4} \end{cases} \tag{1}$$

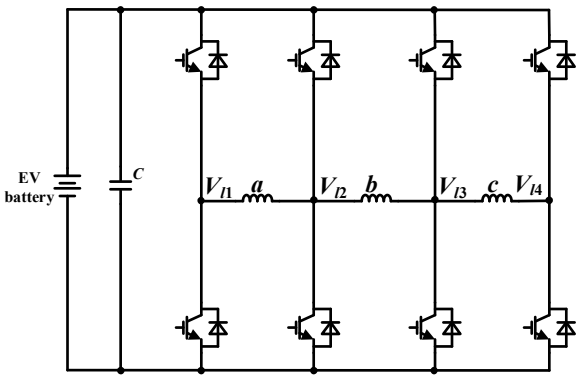


Fig. 1. Series-end winding motor system

$$\begin{bmatrix} V_{l1} \\ V_{l2} \\ V_{l3} \\ V_{l4} \end{bmatrix} = \begin{bmatrix} \cos\theta_e & -\sin\theta_e & 3/2 \\ \cos(\theta_e - 2\pi/3) & -\sin(\theta_e - 2\pi/3) & 1/2 \\ \cos(\theta_e + 2\pi/3) & -\sin(\theta_e + 2\pi/3) & -1/2 \\ \cos\theta_e & -\sin\theta_e & -3/2 \end{bmatrix} \begin{bmatrix} V_{ld} \\ V_{lq} \\ V_0 \end{bmatrix} \quad (2)$$

$$\begin{bmatrix} V_{ld} \\ V_{lq} \end{bmatrix} = \frac{1}{2} \begin{bmatrix} 1 & 1/\sqrt{3} \\ -1/\sqrt{3} & 1 \end{bmatrix} \begin{bmatrix} V_d \\ V_q \end{bmatrix} \quad (3)$$

Another method to convert phase voltage to line voltage is conducted as (4). This method makes full use of the DC voltage and prevent the occurrence of over-modulation.

$$\begin{cases} V_{l1} = V_a + V_b + V_c - V_{CM}/2 \\ V_{l2} = V_b + V_c - V_{CM}/2 \\ V_{l3} = V_c - V_{CM}/2 \\ V_{l4} = -V_{CM}/2 \end{cases} \quad (4)$$

where $V_{CM} = \max\{V_a, V_b, V_c\} + \min\{V_a, V_b, V_c\}$.

In this paper, zero-sequence current is used to generate AC excitation on battery current. Therefore, it is necessary to ensure that the zero-sequence current is controlled to be zero before the proceeding. A proportional-integral-resonant (PIR) controller with a resonant frequency of the fundamental frequency and the third harmonic of the motor is utilized to control the zero-sequence current 0. For the desired zero-sequence current, another independent proportional-resonant (PR) controller is used for control, whose resonance frequency is the same as the frequency of the desired zero-sequence current. When the desired zero-sequence current includes multiple frequency components, the resonance frequency of the PR controller should meet the requirements of all frequency components of the current.

### *B. Excitation current analysis*

Zero-sequence current does not contribute to the torque of the motor, so it has little effect on normal operation. The superposition of zero-sequence currents can lead to changes in the zero-sequence magnetic field and ohmic losses. Based on the principle of energy conservation, the voltage and current relationship between the DC side and the AC side is established as (4). $P_{dc}$ is power from DC side. $P_{out}$ is electromagnetic power. $P_{ohmic}$ is ohmic losses on motor windings. $E_{magnetic}$ is the energy stored in the motor. Other power losses such as switch loss are in $P_{other}$.

$$P_{dc} = P_{out} + P_{ohmic} + \frac{dE_{magnetic}}{dt} + P_{other} \quad (4)$$

Since the excitation current is an AC signal, (4) is differentiated to obtain (5). The battery voltage fluctuations are ignored because they are extremely small. $P_{out}$ and $P_{ohmic}$ are also considered constant. $R_s$ is phase resistor. $L_0$ is zero-sequence inductor.

$$\begin{aligned} V_{dc}\frac{di_{dc}}{dt} &= R_s \frac{d\left[(i_a + i_0/3)^2 + (i_b + i_0/3)^2 + (i_c + i_0/3)^2\right]}{dt} \\ &+ \frac{d^2(E_d + E_q + E_0)}{dt^2} \\ &= \frac{R_s}{3}\frac{di_0^2}{dt} + \frac{L_0}{2}\frac{d^2 i_0^2}{dt^2} \end{aligned} \quad (5)$$

1) Single frequency

When the excitation is a sine wave of a single frequency, $i_0 = I_m \sin\omega t$, the AC excitation generated on the DC side can be deduced as (6).

$$\begin{aligned} \tilde{i}_{dc} &= -\frac{I_m^2 R_s}{6V_{dc}}\cos 2\omega t + \frac{\omega I_m^2 L_0}{2V_{dc}}\sin 2\omega t \\ &= A\sin(2\omega t + \theta) \end{aligned} \quad (6)$$

The frequency of excitation current on DC side is two times of $i_0$, the amplitude is proportional to square of $i_0$ amplitude. When the frequency is low, the current excitation is caused by ohmic losses. When the frequency increases, the current excitation is mainly caused by the fluctuation of the zero-sequence magnetic field energy, and the amplitude of the excitation current is approximately proportional to the excitation frequency.

2) Multiple frequency

When $i_0 = \sum_{k=1}^{n} I_{mk}\sin(\omega_k t + \theta_k)$, the excitation current contains up to $n^2$ frequencies as (7).

$$\tilde{i}_{dc} = \sum_{i=1}^{n^2} A_i \sin(\omega_i t + \theta_i) \quad (7)$$

$\omega_i$ is twice the injection frequency ($2\omega_1$, $2\omega_2$,...,$2\omega_n$) or the sum and difference of different frequencies ($\omega_1 \pm \omega_2$, $\omega_1 \pm \omega_3$,...,$\omega_1 \pm \omega_n$,..., $\omega_{n-1} \pm \omega_n$, assuming $\omega_1 > \omega_2 > ... > \omega_n$). This approach consumes significantly less time than single frequency excitation. This method requires adjusting the amplitude and phase of each frequency component to avoid cancellation and ensure that the signal amplitude is not too low at the desired frequency.

### *C. Impedance calculation*

When the generated excitation is a single frequency, the impedance modulus and impedance angle at that frequency are obtained by dividing the generated voltage and current. When the generated excitation is multi-frequency, a frequency decomposition (usually using FFT) is required before calculating the impedance parameters based on the voltage and current of the corresponding frequency. [1] The impedance of each frequency is calculated by (8).

$$Z_\omega = \frac{\dot{U}_\omega}{\dot{I}_\omega} \quad (8)$$

## III. SIMULATION AND EXPERIMENT

### *A. Simulation*

Simulation is carried out in MATLAB/Simulink. A three-phase salient permanent magnet synchronous motor model is used in the simulation. The high-voltage battery pack is replaced by a voltage source in series with R-RC Thevenin equivalent circuit (Fig. 2) to verify the correctness and feasibility of the method. The parameters are listed in TABLE I.

TABLE I
SIMULATION PARAMETERS

| PARAMETERS | VALUES |
|---|---|
| $L_d$ | 1.5mH |
| $L_q$ | 3.0mH |
| $L_0$ | 1.0mH |
| $R_s$ (phase resistor) | 83mΩ |
| $p$ (pole pairs) | 8 |
| $R_{ser}$ | 5mΩ |
| $R_{ct}$ | 5mΩ |
| $C_{nf}$ | 3F |
| $V_{dc}$ | 100V |
| $C_{dc}$ | 30mF |
| $f_s$ (switch frequency) | 10kHz |

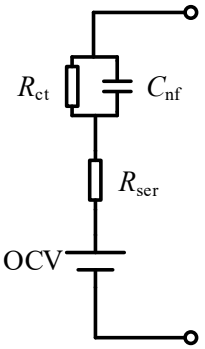

Fig. 2. Thevenin circuit of voltage source

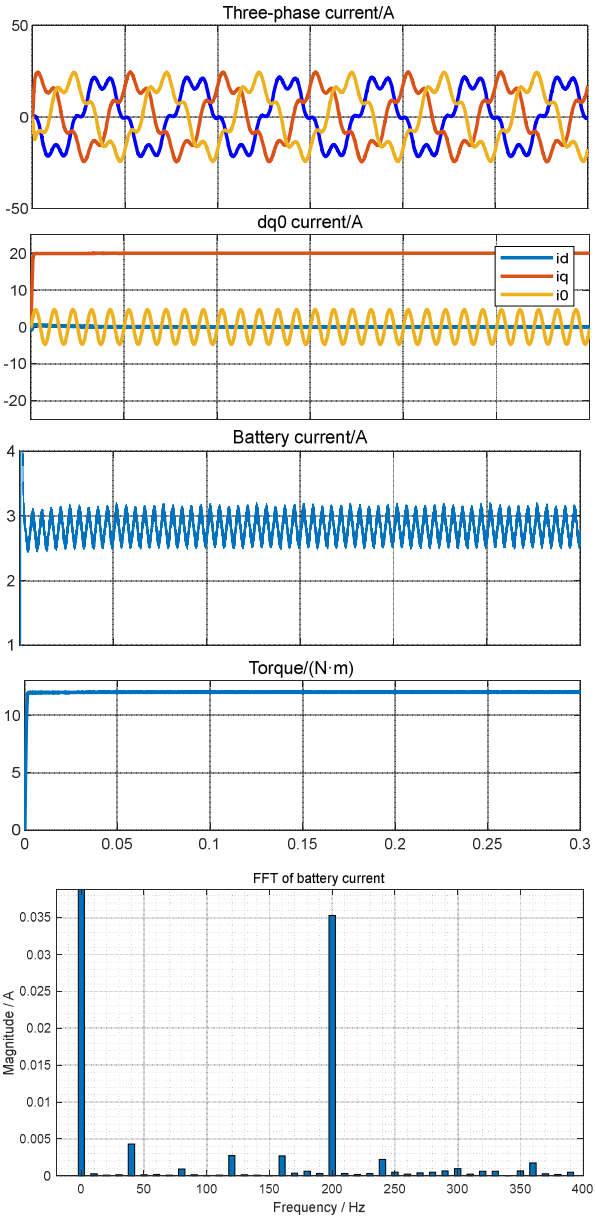

Fig. 3. Single frequency excitation

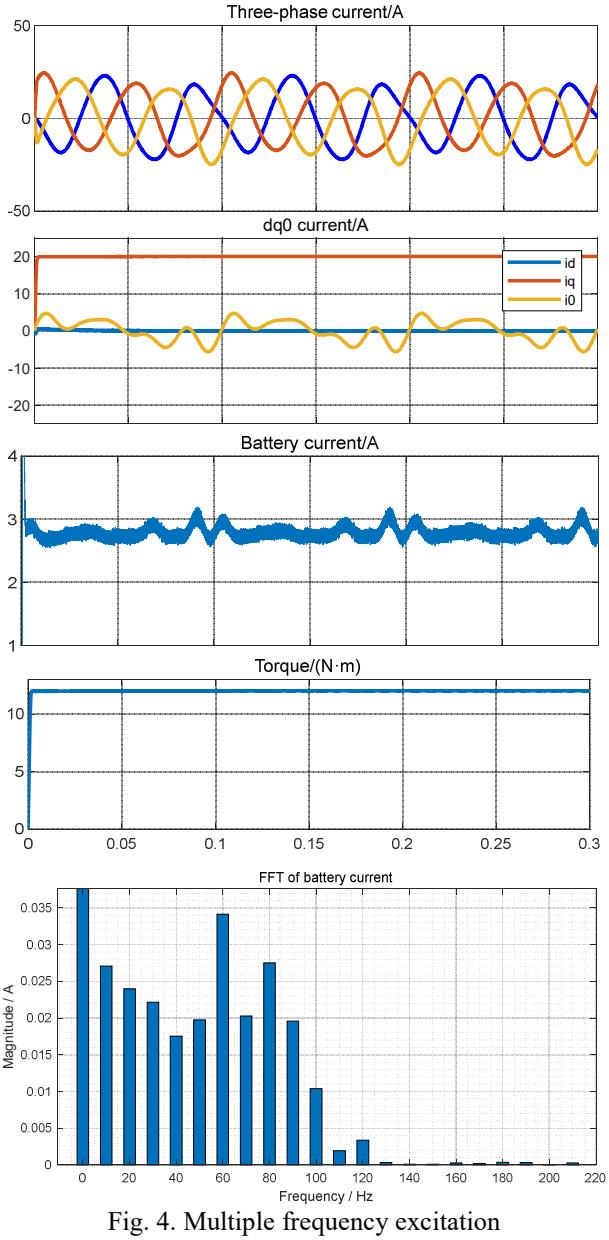

Fig. 4. Multiple frequency excitation

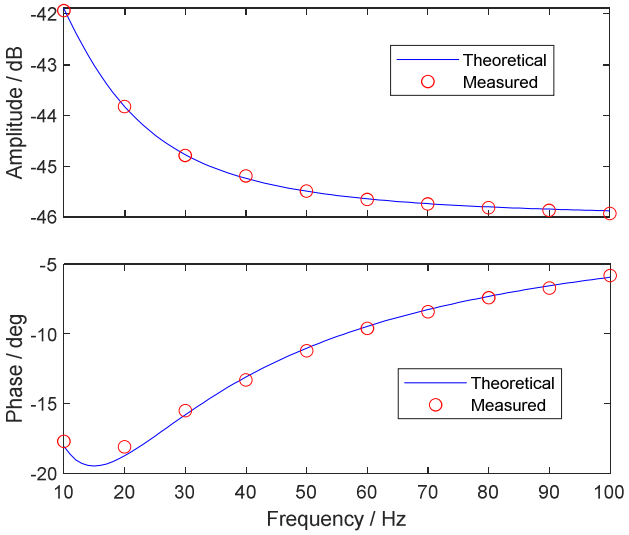


Fig. 5 Magnitude and phase frequency characteristic curves of identification results versus theoretical values

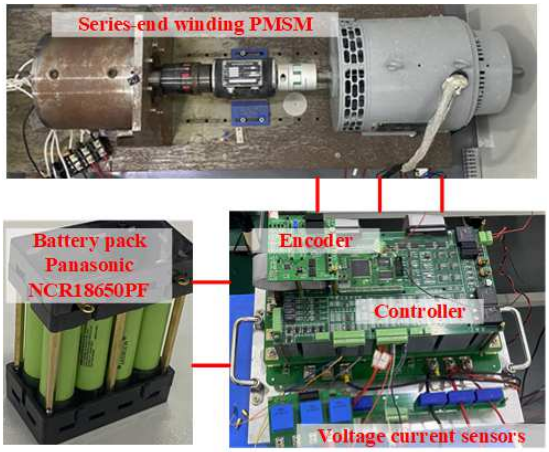


Fig. 6 Experiment platform

The excitation current is injected when the motor three-phase current frequency is stabilized at 20Hz, $i_q$ = 20A and $i_d$ = 0. Single frequency and multiple frequency excitation are carried out respectively. The three-phase current, dq0 current, current of battery, and torque are shown in Fig 3 and 4. In Fig.3 the excitation signal frequency is 100Hz, $i_0 = 5\sin 200\pi t$ A, and in Fig 4, the excitation is the superposition of 10Hz, 30Hz, 40Hz and 50Hz, $i_0 = 2\sin 20\pi t + 1.5\sin 60\pi t + 1.4\sin 80\pi t + 1.2\sin(100\pi t + \pi/4)$ Frequency distribution of battery current is also presented in Fig. 3 and Fig. 4. As can be seen in Fig 4, only four frequencies need to be injected to obtain 10Hz, 20Hz to 100Hz, 10 frequency components on the DC side. Fig 5 shows the curves of the magnitude/phase-frequency characteristics of the battery model calculated by the excitation signal and the theoretical curves. The results are in good agreement with the theoretical values.

TABLE II
EXPERIMENT PARAMETERS

| Parameters | Values |
|---|---|
| $L_d$ | 0.92mH |
| $L_q$ | 1.75mH |
| $L_0$ | 0.65mH |
| $R_s$ (phase resistor) | 78mΩ |
| $p$ (pole pairs) | 4 |
| Switch frequency | 10kHz |
| Cells in a battery pack | 8 |
| Battery packs in series | 3 |
| Cell nominal voltage | 3.6V |
| Nominal capacity | 2900mAh |

### B. *Experiment*

Experiment is carried out on a series-end winding PMSM as Fig 6 shows. The controller is TMS320F28377D from Texas Instrument. Battery pack is constructed by NCR18650PF from Panasonic. Parameters are in TABLE II. In the experiment, an excitation synchronous motor is controlled as a linear load for the series-end PMSM.

In the experiment, the motor control program is first initiated. The fundamental frequency of the motor is stabilized at 25Hz, namely the speed is 375rpm. The motor speed is stable, and the control performance is good. Zero-sequence current is controlled zero. $I_d$ is controlled zero and $I_q$ is 4A. After the motor reaches steady state, frequency scan starts, and a series of frequencies are injected into the motor zero-sequence from low to high. The first frequency injected into the battery is 1Hz, corresponding to a zero-sequence current frequency of 0.5Hz. To ensure the sinusoidal current reaches steady state, the zero-sequence current at 0.5 Hz was injected for a total of four cycles. After that, frequencies from 1Hz to

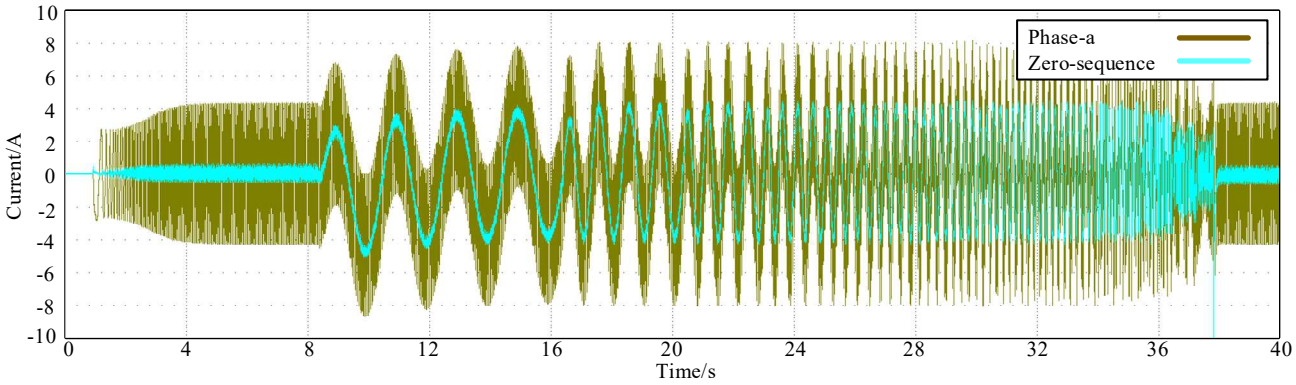

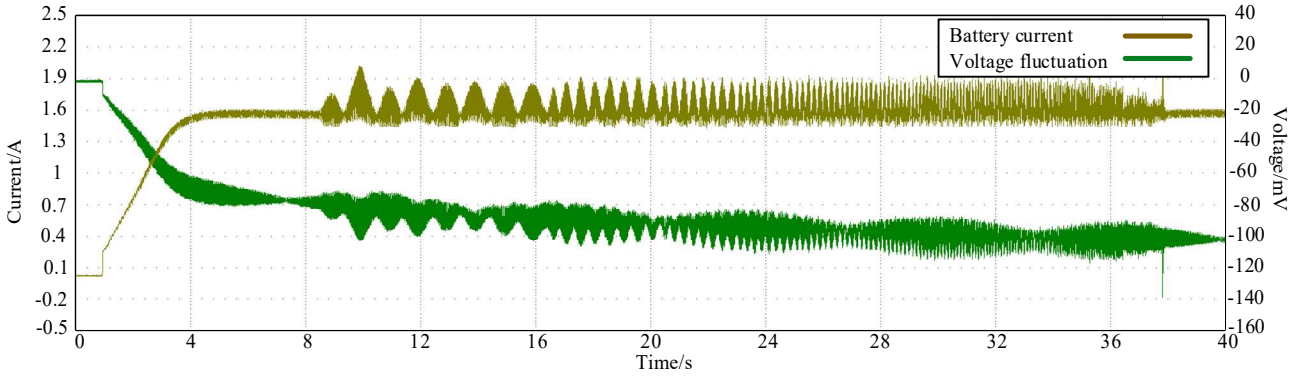


4.5Hz were injected into the motor zero-sequence current in sequence following the same method. For frequency of 5Hz, due to the shorter period, more injection cycles are required to reach stability. So, for frequencies from 5Hz to 25Hz, every 5Hz a frequency point is taken, and 15 cycles of AC excitation are injected at each frequency point. During the injection process, the amplitude of the zero-sequence current was kept at 4A. One frequency characteristic scan from 1Hz to 50Hz has been completed for the battery by now.

Fig.7 and Fig. 8 presents the current and voltage of the process. The motor started and reached steady state in three seconds, followed by four seconds of stable operation before beginning AC excitation injection. The entire frequency scanning process lasts for about 30 seconds. The expected AC excitation signal was successfully injected by measuring the voltage and current of the battery.

However, at zero-sequence current of 25Hz, which is close to the frequency of motor base current, the current fluctuation occurs, So the measurement of 50Hz is incorrect. This may be due to the fact that the zero-sequence impedance of the motor is very small, which makes it difficult to stabilize the control. In voltage and current measurement, due to the switching operation of the IGBT, high-frequency voltage and current pulses are generated, which lead to electromagnetic interference. These pulses generate harmonics, resulting in high-frequency noise on the DC bus.

Figures 9 and 10 show the Bode plot and Nyquist plot of the online impedance characteristics of the experimental battery, respectively, as measured in the experiment. Restricted by the frequency range, the Nyquist plot draws a quarter circle of the plot. And because of the high-frequency noise from the inverter, there is uncertainty of the impedance measurement. But overall, it matches the theoretical impedance curve of the battery.

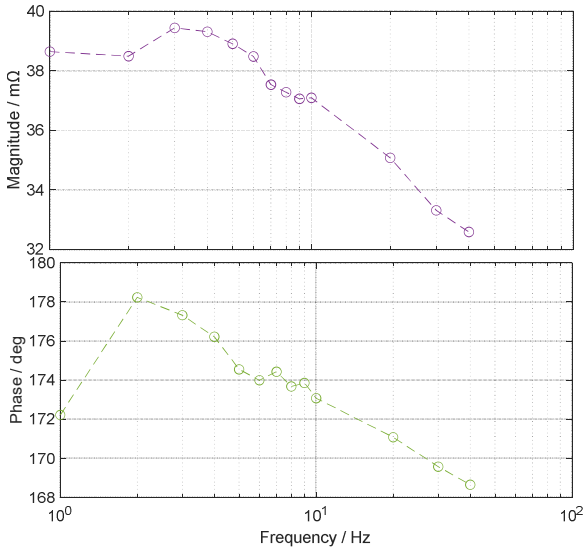


Fig. 9 Bode plot of battery impedance

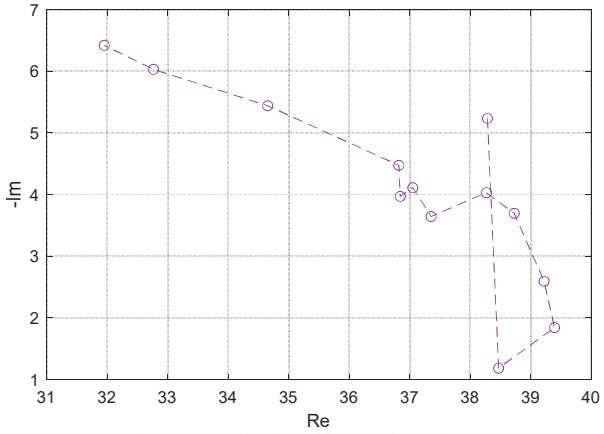


Fig. 10 Nyquist plot of battery impedance

## IV. Conclusions

In this paper, a method for battery impedance online identification excitation signal injection using motor zero sequence current is proposed. It is possible to generate AC signals of any frequency on the DC side without adding additional excitation devices. By simply controlling the inverter through software, and collecting and processing the voltage and current of the battery pack or battery cell, the online impedance parameters of the battery can be obtained. The simulation and experiment results consist with the theory analysis.

This approach can be easily extended to motor drive topologies with zero-sequence current control capability such as open-end winding motor. One of the problems is that the voltage fluctuations are quite small, and the measurement of voltage requires a high degree of accuracy. The zero-sequence current injection can affect the output voltage of the inverter, so in high speed or heavy load the injection needs to be conducted carefully. High-frequency

noise from the inverter during the operation adds to the uncertainty of the measurement, which should be eliminated. In the future, it is worthwhile to study how to choose the amplitude of the injected signal so that the error of impedance identification can be further reduced. The relationship between the online impedance of the battery and the battery state also needs to be further investigated.

## REFERENCES


[1] X. Wang, X. Wei, J. Zhu, H. Dai, Y. Zheng, X. Xu, Q. Chen, "A Review of Modeling, Acquisition, and Application of Lithium-ion Battery Impedance for Onboard Battery Management," eTransportation, Volume 7, 2021, 100093, ISSN 2590-1168, doi.org/10.1016/j.etran.2020.100093.

[2] D. A. Howey, P. D. Mitcheson, V. Yufit, G. J. Offer and N. P. Brandon, "Online Measurement of Battery Impedance Using Motor Controller Excitation," in IEEE Transactions on Vehicular Technology, vol. 63, no. 6, pp. 2557-2566, July 2014, doi: 10.1109/TVT.2013.2293597.

[3] S. K. Dam and V. John, "High-Resolution Converter for Battery Impedance Spectroscopy," in IEEE Transactions on Industry Applications, vol. 54, no. 2, pp. 1502-1512, March-April 2018, doi: 10.1109/TIA.2017.2771498.

[4] E. Din, C. Schaef, K. Moffat and J. T. Stauth, "A Scalable Active Battery Management System With Embedded Real-Time Electrochemical Impedance Spectroscopy," in IEEE Transactions on Power Electronics, vol. 32, no. 7, pp. 5688-5698, July 2017, doi: 10.1109/TPEL.2016.2607519.

[5] Varnosfaderani, M.A. and Strickland, D., Online impedance spectroscopy estimation of a dc–dc converter connected battery using a switched capacitor-based balancing circuit. The Journal of Engineering, 2019: 4681-4685. https://doi.org/10.1049/joe.2018.8069

[6] X. Wang, X. Wei, Q. Chen and H. Dai, "A Novel System for Measuring Alternating Current Impedance Spectra of Series-Connected Lithium-Ion Batteries With a High-Power Dual Active Bridge Converter and Distributed Sampling Units," in IEEE Transactions on Industrial Electronics, vol. 68, no. 8, pp. 7380-7390, Aug. 2021, doi: 10.1109/TIE.2020.3001841.

[7] A. Li, D. Jiang, W. Kong and R. Qu, "Four-Leg Converter for Reluctance Machine With DC-Biased Sinusoidal Winding Current," in IEEE Transactions on Power Electronics, vol. 34, no. 5, pp. 4569-4580, May 2019, doi: 10.1109/TPEL.2018.2864244.